Chemical Science

Accepted Manuscript

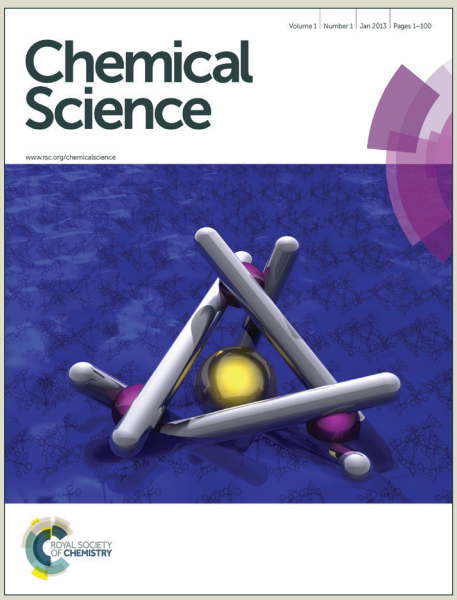

ROYAL SOCIETY OF CHEMISTRY

www.rsc.org/chemicalscience

Stimuli-Responsive Hybrid Materials: Breathing in Magnetic Layered Double Hydroxides Induced by a Thermoresponsive Molecule

Gonzalo Abellán,[a†] Jose Luis Jordá,[b] Pedro Atienzar,[b] María Varela,[c,d] Miriam Jaafar,[e,f] Julio Gómez-Herrero,[e,f] Félix Zamora,[e,g] Antonio Ribera,[a] Hermenegildo García[,b] Eugenio Coronado[*,a]*

[a] *Instituto de Ciencia Molecular, Universidad de Valencia, Catedrático José Beltrán 2, 46980, Paterna, Valencia, Spain.*

[b] *Instituto de Tecnología Química (UPV-CSIC). Universidad Politécnica de Valencia – Consejo Superior de Investigaciones Científicas, Avenida de los Naranjos s/n, 46022, Valencia, Spain.*

[c] *Oak Ridge National Laboratory, Materials Science and Technology Division, Oak Ridge, TN 37830-6071, USA.*

[d] *Universidad Complutense de Madrid, Dpt. Fisica Aplicada III & Instituto Pluridisciplinar, Madrid 28040, Spain.*

[e] *Centro de Investigación de Física de la Materia Condensada, Universidad Autónoma de Madrid, 28049, Madrid, Spain.*

[f] *Departamento de Física de la Materia Condensada. Universidad Autónoma de Madrid. E-28049 Madrid, Spain.*

[g] *Departamento de Química Inorgánica. Universidad Autónoma de Madrid, 28049 Madrid, Spain.*

† Current address: Department of Chemistry and Pharmacy and Institute of Advanced Materials and Processes (ZMP), University Erlangen-Nürnberg, Henkestr. 42, 91054 Erlangen and Dr.-Mack Str. 81, 90762 Fürth, Germany.

* e-mail: hgarcia@qim.upv.es (H. G.), eugenio.coronado@uv.es (E.C.).

Keywords: photochemistry, azo compounds, magnetic properties, layered compounds, host-guest systems

Abstract

A hybrid magnetic multilayer material having micrometric size, highly crystalline hexagonal crystals consisting on CoAl–LDH ferromagnetic layers intercalated with a thermoresposive 4-(4-anilinophenylazo)benzenesulfonate (AO5) molecules diluted (ratio 9:1) with a flexible sodium dodecylsulphate (SDS) surfactant has been obtained. The resulting material exhibits thermochromism attributable to the isomerization between the azo (prevalent at room temperature) and the hydrazone (favoured at higher temperature) tautomers, leading to a thermomechanical response. In fact, these crystals exhibited thermally induced motion triggering remarkable changes in the crystal morphology and volume. *In situ* variable temperature XRD of these thin hybrids shows that the reversible change into the two tautomers is reflected in a shift of the position of the diffraction peaks at high temperatures towards lower interlayer spacing for the hydrazone form, as well as a broadening of the peaks reflecting lower crystallinity and ordering due to non uniform spacing between the layers. These structural variations between room temperature (*BS* = 25.91 Å) and 100 ºC (*BS* = 25.05 Å) are also reflected in the magnetic properties of the LDH due to the variation of the magnetic coupling between the layers. Overall, our study constitutes one of the few examples showing a fully reversible thermo-responsive breathing in a 2D hybrid material. In addition, the magnetic response of the hybrid can be modulated due to the thermotropism of the organic component that, by influencing the distance and in-plane correlation of the inorganic LDH, modulates the magnetism of the CoAl–LDH sheets in a certain range.

Introduction

Multifunctionality is one of the hot topics in chemical and materials science. The so-called hybrid approach has been revealed as a fruitful route to design multifunctional materials in which each one of the two constituent networks brings one property to the

solid.[1–4] Even more appealing is the case in which both components are coupled as new properties arise from their mutual interaction. Along this front, stimuli-responsive materials, in which some properties can be tuned by external stimuli are attracting considerable interest in view of their applications as chemical switches, memories, or molecular sensors.[5–7] An emerging class of such materials are those exhibiting reversible cycling (breathing). Apart from some composite materials based on hydrogels[8], chemistry provides nice examples of crystalline breathing materials in the field of MOFs.[9,10] Exciting examples like volumetric negative thermal expansion[11] or massive anisotropic thermal expansion[12] have been very recently reported, paving the way for a plethora of possible applications in sensing,[13] magnetic switching,[14,15] heat storage/transfer,[16] or for temperature switchable devices.[17,18]

Another class of chemically-designed materials that can be suitable for breathing are those formed by inorganic layers, as they can host responsive molecules in the interlamellar space that can change their volume. Still, the examples of this class are limited to photoresponsive layered silicates[19–23] and their characterization is limited to study the X-ray diffraction patterns and the absorption and fluorescence spectra.[24,25] Recently, Inoue and co-workers reported the only example based on inorganic niobate nanosheets that exhibits macroscopic morphological change originated by reversible photoinduced sliding of the layers.[26] In view of these results we became interested in studying the more versatile layered double hydroxides (LDHs) as they offer a broad range of possibilities to develop responsive materials that are almost unexplored at the present.[27–29] These layered hosts display brucite-like structure composed by positively charged sheets consisting in edge-shared $M(OH)_6$ octahedra. Moreover, through the rational choice of the transition metals, magnetic layers could be easily obtained[30,31] in which their magnetic properties can be conveniently tuned by modifying the interlayer

distance.[32] Taking advantage of this feature we have recently shown that, by inserting in the interlamellar space of a ferromagnetic CoAl–LDH azobenzene-4,4'-dicarboxylate molecules that respond to a light stimulus changing its size, the magnetic properties of the LDH hybrid can be reversibly switched.[33] Apart from this example, we are not aware of other works dealing with the reversible photo-switching of micrometric LDH systems. In that example azobenzene-4,4'-dicarboxylate is connected through the two extremes to the layers leading to a "rigid" system in which the *cis-trans* photoinduced isomerization is almost unable to change the interlayer distances; in turn, it produces a sharp tension within the layers including distortion, which seems to be the responsible for the significant changes observed in the magnetic properties. Here we will explore the use of a photoactive molecule, which is designed to be connected by one of the two extremes to the host system. This modification is expected to lead to more flexibility to the prepared material as in this case a sliding of the layers may take place (**Figure 1**).

FIGURE 1

As switching molecule we have chosen the thermochromic 4-(4-anilinophenylazo)benzenesulfonate (AO5) molecule, which exhibits upon heating at moderate temperatures a reversible change in the structure due to a tautomeric equilibrium (**Figure 2**). The resulting hybrid shows temperature-responsive breathing, with drastic structural transformations. As demonstrated by means of variable temperature PXRD, AFM and magnetic measurements, this layered hybrid molecular system exhibits a reversible morphological change, and can be considered as a thermoactivated responsive material.

FIGURE 2

Results and discussion

A CoAl–CO_3 material with very high crystallinity and well-defined hexagonal morphology was herein obtained by means of a modified homogeneous precipitation method using urea as ammonia releasing reagent (ARR) and subsequently, submitted to ion exchange to obtain the NO_3^- form (**Figure SI1**). To gain further insight on the microstructure of the initial platelets, we analysed the sample by aberration-corrected STEM-EELS at 60 kV. The crystals were in the range of microns in size, as depicted in the low magnification HAADF image of **Figure 3** (left). An atomic resolution high angle annular dark field (HAADF) STEM image of the CoAl sample is shown on the right panel, acquired with the electron beam perpendicular to the platelet plane. The sample is highly crystalline and a clear hexagonal atomic structure can be observed with well-defined edge-sharing metallic octahedra that clearly indicate the brucite-like structure of the layers (see the Fourier transform in the inset). Some stacking faults are also observed with occasional lack of periodicity in the atomic chains, probably related to some disruptions in the cation ordering of the samples.[31,34,35] Unfortunately, the samples were quite sensitive to electron beam irradiation and did damage too fast under the electron beam to acquire meaningful spectroscopic data that would allow a detailed chemical quantification.

FIGURE 3

FIGURE 4

For the preparation of the thermoresponsive hybrids, a co-intercalation of two organic anions has been developed. This approach was already used to prepare ZnAl–LDH thermochromic hybrids containing AO5 and sodium benzene dodecyl sulfonate in the intergallery space.[36] We have diluted the thermochromic AO5 molecule with a

surfactant (SDS) in order to provide a flexible hydrophobic environment, making possible the operation of a reversible cycle between the azo and the hydrazone tautomeric forms of the thermoresponsive azocompound. The synthesis of the ferromagnetic CoAl–AO5 LDH hybrids has been carried out by nitrate-exchange under mild conditions. Specifically, the CoAl–NO_3 was modified by co-incorporation of sulfate dodecyl and AO5 molecules in the appropriate SDS/AO5 ratio to achieve the optimal tautomeric behaviour (*i.e*. 9:1). In this sense, the SDS plays a crucial role minimizing aggregation of dye molecules that would result in self-quenching of the tautomerism, as recently reported by Xu and co-workers.[37] On the other hand, we have selected the 2:1 metal ratio (Co:Al) in order to maximize the trivalent metal content, which results in an enhanced restriction of dye mobility. It is worth mentioning the high crystallinity of the final hybrid material, as depicted in **Figure 4**.

Chemical analysis and infrared spectroscopy confirm the absence of carbonates and nitrates indicating that the ion exchange steps have been performed completely. Moreover, CoAl–AO5 was characterized by thermogravimetric analysis under air atmosphere (**Figure SI2**). There was an initial loss of desorption of water corresponding to weakly physisorbed water (T < 200 ºC). After this initial weight loss, a considerable multi-step jump of about 25 % attributable to elimination of chemisorbed interlamellar water and combustion of organic anions takes place in the temperature range from 200 ºC to 500 ºC.

Field emission scanning electron microscopy (FESEM) provides images showing the hexagonal morphology of the LDHs (**Figure 5**). Well-developed hexagonal crystals of about 4.5 μm diagonal were determined for both the CoAl–NO_3 and CoAl–AO5 LDHs. Moreover, a precise correlation between the thickness of the platelets and their composition has been observed (**Figure SI3**). In fact, while the hexagonal morphology

was retained, the thickness of the platelets increased by the anion exchange from NO_3^- to AO5/SDS. The ratio of the average particle thickness (from 71 to 197 nm; 2.8 times) before and after the exchange of NO_3^- with the AO5/SDS mixture was consistent with the ratio of the basal spacing (from 0.88 to 2.59 nm; 2.9 times) before and after the anion exchange determined by PXRD. These measurements confirm the topochemical reaction of the intercalation, as recently reported by Ogawa *et al*.[38]

FIGURE 5

This platy morphology of CoAl–AO5 is especially suited for the preparation of thin films coating flat substrates. These films were obtained by spraying a paste of CoAl–AO5 suspended on acetyl acetonate using α-terpineol and carboxymethyl cellulose as thickener, followed by evaporation of these additives. Profilometric analyses of these films are shown in **Figure SI4** that also shows a photograph of the films on high-quality suprasil quartz. As it can be seen in this Figure, the film is highly homogeneous without formation of pinholes, cracks or crevices on it. The average thickness is around 1.5 μm.

These films have allowed us to perform a spectroscopic study of the reversible photochromism exhibited by CoAl–AO5. Heating of the film from room temperature to > 65 ºC produces a significant visual change in the color from yellow to red.

This change can be quantified by the corresponding variation in the UV-Vis absorption spectrum of the material (**Figure 6**). The fact that the CoAl–AO5 material is in the form of thin film, allows recording absorption spectra by transmission mode, a technique that is not possible working with opaque powders. The state exhibiting yellow color has an absorption band at λ_{max} = 365 nm that has been attributed to the azo tautomer (*A*) of AO5. Upon heating, a broader band at longer wavelengths (λ_{max} = 465 nm) that has been ascribed to the hydrazone form of AO5 (*H*) develops.[39] This change in color was

reversible and is compatible with the proposed shift in the equilibrium between the two forms of AO5 as depicted in **Figure 2**. Parallel to the changes in the UV-Vis absorption spectra, changes in fluorescence spectroscopy are detected.

FIGURE 6

Although the emission from the material is weak due to the transparency and thinness of the film, photoluminescence was observed both for the yellow AO5–*A* and the red AO5–*H*. At room temperature excitation with light of 370 nm gives an emission peaking at about 550 nm. When the film is heated, and the 465 nm band develops, the photoluminescence shifts to the red exhibiting the maximum at 585 nm. **Figure 6** illustrates the changes in the emission spectra accompanying to the variation in the absorption spectra.

In order to provide some additional spectroscopic data to understand the changes occurring in the absorption optical spectra of the CoAl–AO5 material, we undertook a study of the UV-Vis absorption spectra of pure AO5 molecules in solution as well as some laser flash transient spectroscopy. While in acetonitrile solution compound AO5 exhibit a band with absorption maximum at 463 nm (**Figure SI5**), in aqueous solution the absorption maximum in the range of pH values from 3 to 10 was between 465 nm (acid pH) to 450 (basic pH). According to these spectra it seems that the tautomerization observed upon heating and cooling is related to changes with the polarity of the tautomeric equilibrium of AO5 between *A* and *H*, as previously suggested.[36] In fact, when an acid aqueous solution (pH = 3) of AO5 (λ_{max} = 465 nm) is photolyzed with 355 nm laser pulse under argon atmosphere, generation of a lived long transient with a characteristic band at 530 nm is observed (**Figure SI6**). This transient observed in water with characteristic λ_{max} red-shifted with respect to the absorption of the starting isomer

is compatible with the generation of the *cis* isomer of the azo compound that is a general photochemical transformation of azo compounds.[40,41] Observation of this *cis* isomer at 530 nm seems to rule out the involvement of this isomer in the reversible thermal changes observed for the CoAl–AO5 material. Therefore, in view of the previous proposal on the occurrence of *A* to *H* reversible thermal tautomerisation for AO5 and our observation of a band at 530 nm upon photolysis of AO5, the most likely rationalization for the changes observed in the optical spectrum upon heating is, then, the conversion between the *A* and the *H* forms of AO5.

The most relevant feature of CoAl–AO5, related to the reversible thermochromism attributable to the mesomeric proton shift, is the change in the spacing between the layers that accompanies the reversible tautomerization from the *A* to *H* forms. X-ray diffraction of CoAl–AO5 at room temperature gives the characteristic pattern expected for highly crystalline LDH with up to eight sharp (00*l*) diffraction peaks, presenting a *BS* of 25.91 Å, slightly smaller than that previously reported for SDS intercalated LDHs, as a consequence of the incorporation of the AO5 molecules.[38,37]

We were interested in determining if the reversible changes into the two isomeric forms that presumably should have different molecular dimensions are reflected also in changes into the structure, *i.e*. the interplanar distance of LDH. The study was performed with thin films of CoAl–AO5 supported on a platinum holder. We followed the changes in the high temperature chamber upon heating from room temperature to 100 ºC. The configuration of the cell holder for thin films did not allowed to monitor 2θ angles smaller than 5º and, therefore, the first (00*l*) peak was not observable in the measurement. It was observed that also for these films the diffraction pattern changes shifting the position of the (00*l*) peaks towards higher angles as well as the peaks become broader. The broadening should indicate a more disordered stacking of the

layers in CoAl–AO5. Based on recent similar finding for niobate[23,26] we propose that this disorder should be a consequence of a random sliding of the constituting hydroxide layers (*vide infra*), a fact that is triggered by the partial isomerization of *A* into *H* forms leading to a distribution of interlayer distances around a maximum value. These changes were reversible upon heating and cooling cycling, in accordance with the changes previously observed in transmission absorption spectroscopy for the isomerism between the azo and hydrazone forms. **Figure 7** shows a series of X-ray diffraction patterns collected at 25 or 100 ºC illustrating the changes observed. While for room temperature the position of the (006) peaks is around 6.8º, at 100 ºC the broader peak has the maximum shifted towards higher values in 2θ, corresponding with a slight change in the basal spacing from 25.91 to 25.05 Å (**Figure 8**). In this sort of hybrid materials, the presence of water molecules in the interlayer space is controlled by the different hydrophobic-hydrophilic contributions of the amphiphilic surfactant molecules, the dye and the LDH layers.[37] The assumption that the mechanism of isomerization by proton shift involves water —probably as shuttle of the protons following a Grotthuss-type proton migration mechanism, as previously proposed (**Figure SI7**)[36,42]— is reflected by the fact that this cycling between the two diffraction patters shown in **Figure 8**, can also be achieved by submitting the cell chamber to vacuum to desorb water and, then, exposing the sample to moist air. It is worth to comment that if instead of moist air, dry nitrogen is introduced into the chamber, the position of the peaks remain as in vacuum at 2θ value of *ca*. 7.1º. These changes between moist (006 peak 6.7º) and dry (006 peak 7.1º) states were also reversible as already observed for thermochromism and for the heating in XRD.[43] In addition, a control experiment consisting on a CoAl–LDH intercalated only with SDS molecules (CoAl–SDS) has been performed (**Figure SI8**). In this case, the X-ray diffraction patterns collected at 100 ºC revealed an expansion of

the *BS* after heating (**Figure SI9**), in clear contrast to the thermochromic CoAl–AO5. This interesting phenomenon has been already observed for monometallic layered Zinc hydroxides intercalated with SDS molecules.[44] These experiments allows to ruling out other reasons for the reversible switching like melting of alkyl chains or simple water dehydration induced motion, highlighting the tremendous influence exerted by the inclusion of the thermochromic AO5 molecules.

FIGURE 7

FIGURE 8

Besides XRD and crystallinity we also investigated the variations in the morphology of the CoAl–AO5 crystals by means of a variable temperature AFM, mounted in a standard high vacuum chamber. Heating and cooling were achieved by thermal contact to the sample holder. We prepared a diluted 10^{-3} mg·mL^{-1} ethanol suspension of CoAl–AO5 crystals by sonication and, afterwards, we deposited a drop on a silicon wafer having markers. AFM imaging of the surface revealed platy CoAl–AO5 crystals of reduced dimensions (*ca*. 0.5–1.5 μm) probably due to the sonication. **Figure 9** shows AFM images of one of these crystals acquired at ambient conditions, heating the sample at 80 ºC and then cooled again at RT. In each image we can distinguish a crystal and a reference marker that safely identifies the crystal throughout the experiments. Zoom-in images allow the observation of the evolution of the shape of the particle, exhibiting a pronounced compression upon heating, which is partially reverted freezing to RT.

Moreover, as can be observed in **Figure 9**, the histogram of the volume indicates a decrease in the overall volume of the crystal with heating, which is also partially reversible after freezing. The images clearly reveal notable changes in its morphology and volume, probably due to the random sliding of the hydroxide sheets, in accordance with the broadening and decreased interlayer spacing previously observed in X-ray

diffraction experiments. Furthermore, we have also studied the influence of a drastic dehydration under high vacuum on the sample. This experiment results in the partial destruction of the crystal, which cannot be recovered after exposing to normal conditions (**Figure SI10**). These experiments provide a direct evidence of the thermo-responsive breathing of the hybrid at the microscale as consequence of the isomerization of the AO5 at the nanoscale in the LDH. They also indicate that at the nanoscale these changes in volume are huge (from *ca*. 15 to 25%), and much more pronounced than those predicted from the X-ray diffraction results (performed on bigger crystals of *ca*. 4.5 μm).

FIGURE 9

Another effect of the *A–H* isomerization of AO5 incorporated on LDH is that due to the composition of the CoAl–AO5 LDH, the magnetic response should change reversibly between two states. The precedents showing fully reversible magnetic properties between two states in hybrid materials are scarce,[21,33,45,46] and the reversible structural transformations associated to the thermo-responsive breathing of the crystals should be reflected in changes in their magnetic behaviour. As previously reported, the overall magnetic behaviour of LDH materials depends on the ferromagnetic in-plane superexchange pathways between Co metals and the antiferromagnetic interlayer dipolar interactions, resulting in a low-temperature spin-glass-like behaviour.[33,35,47,48] The reversibility between *A* and *H* forms of the incorporated guest leads to a more disordered state as confirmed by XRD (shift and broadening of the peaks) and AFM (morphological changes) measurements that is in clear contrast to that reported for a CoAl–LDH having intercalated photoisomerizable trans-azobenzene-4,4′-dicarboxylic acid (T1), in which no clear modifications in the XRD peak broadening were observed

after UV irradiation.[33] These structural differences are also reflected in the magnetic behaviour of CoAl–AO5 LDH compared to CoAl–T1 LDH. The magnetic properties of CoAl–AO5 LDH were measured in a SQUID before and after heating of the sample in a quartz capsule at 2 K. On the one hand, *ac* dynamic magnetic measurements, with an applied field of 3.95 G with frequencies oscillating between 1 and 1000 Hz, confirmed the spontaneous magnetization of the hybrid in the three states, showing a clear dependence with the frequency of the oscillating field in both the in-phase and out-of-phase signals, but with no significant differences in the T_M values. Moreover, the thermal variation of χ_m after heating the sample showed almost negligible variations before and after heating (**Figure SI11**). On the other hand, as depicted in **Figure 10**, the hysteresis cycle of the CoAl–AO5 reveals a fully reversible variation of *ca*. 8 % of the saturation magnetization values after heating and cooling the sample. The magnitude of this variation is notably smaller than that reported for the CoAl–T1 (27 %). Otherwise, the coercive field remains almost unaffected (a small change of *ca*. 5 G is observed). In the present case, the very weak change in the magnetic properties of the CoAl–AO5 LDH crystals contrast with the larger changes observed in the more rigid and tensioned CoAl–T1 LDH system, indicating that the magnetic layers remain structurally unchanged during the switching. So, the magnetic changes are exclusively caused by changes in the interlamellar dipolar interactions, which are small.

FIGURE 10

Conclusions

We have described a hybrid multifunctional layered material that makes use of the switching ability of the thermoresponsive 4-(4-Anilinophenylazo)benzenesulfonate molecules to alter the morphology of the material. The different molecular shape of the

azo (stable at room temperature) and the hydrazine (favoured at high temperatures) tautomers is reflected in a variation in the interlayer spacing of the CoAl–LDH material as evidenced by XRD, and this change at the nanoscale has drastic consequences in the microscale, as revealed by AFM. Thus, a large quasi-reversible change in the volume up to *ca*. 25% has been observed correlated to a sliding movement.

As far as the magnetic properties are concerned, one observes that in the present case they are much less affected than in the case in which the functional molecules are bridging adjacent layers. This illustrates how the chemical design of the switching molecules (connected through one side or through the two sides to the layers) affects in different ways the structural magnetic properties of these layered hybrids. This work paves the way for the development of other related "breathing" systems based on LDHs.

Supporting Information

Supporting Information is available.

Acknowledgements

Financial support from the EU (SpinMol Advanced Grant ERC-2009-AdG-20090325), the Spanish Ministerio de Economía y Competitividad (Projects with FEDER cofinancing MAT2011-22785, MAT2012-38567-C02-01, CTQ-2011-26507, Consolider-Ingenio 2010-Multicat CSD2009-00050, and Severo Ochoa Program SEV-2012-0267), Generalitat Valenciana (PROMETEO and ISIC-Nano programs), and VLC/Campus Microcluster "Functional Nanomaterials and Nanodevices" is gratefully acknowledged. This research was sponsored by the Office of Basic Energy Sciences, Division of Materials Sciences and Engineering, U.S. Department of Energy (M.V.).

Electron microscopy was performed at the Centro Nacional de Microscopia Electrónica (UCM) sponsored by the ERC Starting Investigator Award STEMOX#239739. G. A. thanks the EU for a Marie Curie Fellowship (FP7/2013-IEF-627386). P. A. thanks the Spanish MINECO for a Ramón y Cajal Fellowship. We also acknowledge J. A. Carrasco for his help with the experimental work, and J. M. Martínez and G. Agustí for magnetic measurements.

Experimental section

Synthesis

Materials: All chemicals $CoCl_2 \cdot 6H_2O$, $AlCl_3 \cdot 9H_2O$, $NaNO_3$, HNO_3, $CO(NH_2)_2$ (urea), sodium dodecyl sulfate and 4-(4-anilinophenylazo)benzenesulfonate, were used as received from commercial suppliers (Sigma-Aldrich, Fluka and TCI) without further purification. All the experiments were carried out under inert atmosphere to prevent carbonate contamination.

Synthesis of CoAl–CO_3 LDH: $[Co_{0.66}Al_{0.33}(OH)_2](CO_3)_{0.16} \cdot mH_2O$ was synthesized according to the homogeneous precipitation method by using urea as ARR.[49–51] Accordingly, the chloride salts of the metals were dissolved in Milli-Q purged water to reach a total cation concentration of 0.15 M in the final solution and keeping the stoichiometric coefficient constant at a value of $x = 0.33$ (equivalent to a Co/Al molar ratio of 2:1). Next, an aqueous solution of urea (three times the $[Al^{3+}]$) was added. The resulting pink mixture was transferred to a round bottom flask and heated up to 97 °C under reflux conditions. After 48 hours, the resulting finely divided pink powder was filtered, washed thoroughly with distilled water and ethanol, and dried at room temperature under vacuum. The pH value of the remaining solution was found to be around 7.5.

$[Co_{0.66}Al_{0.34}(OH)_2](CO_3)_{0.33}\cdot 0.17H_2O$ Anal. calc. for $H_{2.66}C_{0.33}O_{3.32}N_0C_{o0.66}Al_{0.34}$ (FW = 98.235): H, 2.61; N, 0; C, 1.96. Found: H, 2.58; N, 0.14; C, 1.98.

Preparation of CoAl–NO_3 LDH: $[Co_{0.66}Al_{0.33}(OH)_2](NO_3)_{0.33}\cdot mH_2O$ was obtained by carbonate-exchange of the as-synthesized CoAl–CO_3 LDH in presence of an excess of nitrate anions. In a typical procedure, 1 g of CoAl–CO_3 LDH was immersed in a round-bottom flask containing 1 L of an aqueous solution of $NaNO_3$ (1.5 M) and HNO_3 (0.005 M).[52] This mixture was mechanically stirred under inert atmosphere during 48 h. Afterwards, the resulting pink solid was filtered, washed thoroughly with Milli-Q water and ethanol and dried under vacuum at room temperature.

$[Co_{0.67}Al_{0.33}(OH)_2](NO_3)_{0.33}\cdot 0.31H_2O$ Anal. calc. for $H_{2.62}C_0O_{3.3}N_{0.33}Co_{0.67}Al_{0.33}$ (FW = 108.534): H, 2.42; N, 4.97; C, 0. Found: H, 2.26; N, 3.69; C, 0.18.

4-(4-anilinophenylazo)benzenesulfonate/SDS intercalation, CoAl–AO5: In a typical procedure, 200 mg of CoAl–NO_3 was finely powdered and transferred to a round bottom flask. Then, 45 ml of an aqueous mixture of 4-(4-anilinophenylazo)benzenesulfonate (0.015 M) and SDS (0.14 M), was slowly added under inert atmosphere and continuous stirring. The mixture was sonicated during 5 minutes to produce a homogeneous dispersion and then was vigorously stirred at 900 rpm for 20 h under continuous argon bubbling. Finally, the yellowish precipitate was filtered under inert atmosphere, washed thoroughly with distilled water and ethanol, and dried at room temperature under vacuum.

$[Co_{0.65}Al_{0.34}(OH)_2](C_{18}H_{14}N_3SO_3)_{0.033}(C_{18}H_{29}SO_3)_{0.297}\cdot 0.77H_2O$ Anal. Calc. (FW = 204.401): H, 6.17; N, 0.68; C, 34.87; S, 5.17. Found: H, 5.6; N, 1.24; C, 25.46; S, 5.13

Chemical and Physical Characterization

Carbon, nitrogen and hydrogen contents were determined by microanalytical procedures using an EA 1110 CHNS-O Elemental Analyzer from CE instruments. Metallic atomic

composition of bulk samples was determined by means of electron probe microanalysis (EPMA) performed in a Philips SEM-XL30 equipped with an EDAX microprobe. Atomic resolution studies in real space were carried out by aberration corrected scanning transmission electron microscopy (STEM) and electron energy-loss spectroscopy (EELS) in a Nion UltraSTEM100 operated at 60 kV equipped with a spherical aberration corrector and a Gatan Enfina EEL spectrometer. Samples were prepared by dropping a colloidal suspension of the fresh sample in formamide on a holey carbon-coated copper grid for STEM-EELS observation. Field emission scanning electron microscopy (FESEM) studies were performed on a Hitachi S-4800 microscope operating at an accelerating voltage of 20 kV over metallized (1 min of Au/Pd) samples. Infrared spectra were recorded in a FT-IR Nicolet 5700 spectrometer in the 4000–400 cm^{-1} range using powdered samples diluted in KBr pellets. Thermogravimetric analysis of all compounds were carried out with a Mettler Toledo TGA/SDTA 851 apparatus in the 25–800 °C temperature range under a 10 °C·min^{-1} scan rate and an air flow of 30 mL·min^{-1}. X-ray powder diffraction patterns of the precursor materials were collected with a Bruker D8 Advance A25 X-ray diffractometer, operating at 45 kV and 80 mA Cu-K_α radiation (λ = 1.5406 Å) equipped with a LYNXEYE XE 1-D detector. Profiles were collected in the 2.5° < 2θ < 70° range with a step size of 0.02°. UV-Vis spectra were conducted using a Varian Cary-5G UV-Vis spectrophotometer. Room temperature diffuse reflectance UV-Vis-NIR spectra of solid samples were recorded with a Varian Cary 5000 UV-Vis-NIR scanning spectrophotometer. Steady-state photoluminescence measurements were recorded in a Photon Technology International (PTI) 220B spectrofluorimeter having a 75W Xe arc lamp light excitation and Czerny-Turner monochromator, coupled to a photomultiplier.

Thin films of CoAl–AO5. The films (on quartz Suprasil substrates) were prepared by drop casting on a hot plate (80 ºC) at under ambient conditions a paste of CoAl–AO5 (about 40 mg) in α-terpineol-acetone (1.5 ml of a 1:2 mixture of α-terpineol:acetone) acetyl acetonate using α-terpineol and carboxymethyl cellulose as thickener that was sonicated to obtain a good dispersion. Once the solvent was evaporated the thickness of the layer was measured with an Ambios Xi-100 Non-Contact Optical Profilometer with nanometric vertical resolution. The thickness of the films was about 1 micron.

Irradiations were carried out in situ while the sample was placed on the holder of the spectrometer or XRD difractometer at ambient conditions. XRD patterns of the irradiated samples were obtained using a PANalytical X'Pert PRO diffractometer using copper radiation (Cu K_α = 1.5418 Å) with an X'Celerator detector, operating at 40 mA and 45 kV. Profiles were collected in the $2° < 2\theta < 30°$ range with a step size of 0.017° 2θ. Vacuum and temperature variable experiments were performed in an Anton Paar HTK-1200 high temperature chamber, obtaining pressures of ca. 0.01 Pa. The refinements of the cell parameters of the bulk samples were performed using the FullProf program, considering the R-3m space group.

AFM experiments. Variable temperature Atomic Force Microscope (AFM) images were acquired in dynamic mode using a Nanotec Electronica system operating in the 25–100 ºC temperature range in ambient air conditions. For AFM measurements, Olympus cantilevers were used with a nominal force constant of 0.75 N/m. The images were processed using WSxM. The surfaces used for AFM were marked SiO_2. In order to obtain reproducible results, very flat substrates were used with precisely controlled chemical functionalities, freshly prepared just before the chemical deposition.

AFM Sample preparation: CoAl–AO5 (1 mg) was suspended in 1 mL of EtOH under Ar atmosphere. The resulting suspension diluted to a concentration of about 10^{-3}

$mg \cdot mL^{-1}$. The diluted solution was deposited on SiO_2 (10 μL) by drop casting using a Hamilton syringe. Upon standing 1 h in a homemade Cryocool device, the substrates were dried under an argon flow.

Magnetism experiments. Magnetic measurements were carried out with a Quantum Design superconducting quantum interference device (SQUID) MPMS-XL-5. The susceptibility data were corrected from the diamagnetic contributions of the atomic constituents of the samples as deduced from Pascal's constant tables and the sample holder. The *dc* data were collected under an external applied field of 100 G in the 2–400 K temperature range. Magnetization studies were performed between −5 and +5 T at a constant temperature of 2 K. The *ac* data were collected in the range 2–15 K with an applied alternating field of 3.95 G at different frequencies in the range 1–1000 Hz. The sample was placed on a quartz tube that had been previously measured in the same conditions. In a first run the hysteresis cycle of the magnetization of the sample was measured at 2 K and then the sample was submitted to room temperature and heated with an electrical heater at 100 ºC during several minutes. After this heating, the sample was immediately inserted in the SQUID magnetometer at 100 K and cooled to 2 K in less than 30 min and the hysteresis cycle was repeated. Finally, the sample was submitted again to room temperature during several minutes and measured at 2 K to finish the reversibility measurements. Furthermore, the reproducibility of the measurements was checked for up to three different samples that gave very similar results.

References

1. P. Gómez-Romero and C. Sanchez, in *Functional Hybrid Materials*, eds. P. Gómez-Romero and C. Sanchez, Wiley-VCH Verlag GmbH & Co. KGaA, 2003, pp. 1–14.
2. M. Clemente-León, E. Coronado, C. Martí-Gastaldo and F. M. Romero, *Chem. Soc. Rev.*, 2011, **40**, 473.
3. G. Rogez, C. Massobrio, P. Rabu and M. Drillon, *Chem. Soc. Rev.*, 2011, **40**, 1031.
4. C. Sanchez, P. Belleville, M. Popall and L. Nicole, *Chem. Soc. Rev.*, 2011, **40**, 696.
5. E. Coronado, J. R. Galán-Mascarós, C. J. Gómez-García and V. Laukhin, *Nature*, 2000, **408**, 447–449.
6. E. Coronado and P. Day, *Chem. Rev.*, 2004, **104**, 5419–5448.
7. E. Coronado, C. Martí-Gastaldo, E. Navarro-Moratalla, A. Ribera, S. J. Blundell and P. J. Baker, *Nat. Chem.*, 2010, **2**, 1031–1036.
8. Guo, J.-S. Hu, H.-P. Liang, L.-J. Wan and C.-L. Bai, *Chem. Mater.*, 2003, **15**, 4332–4336.
9. S. Kitagawa and K. Uemura, *Chem. Soc. Rev.*, 2005, **34**, 109–119.
10. G. Férey and C. Serre, *Chem. Soc. Rev.*, 2009, **38**, 1380.
11. D. Dubbeldam, K. S. Walton, D. E. Ellis and R. Q. Snurr, *Angew. Chem. Int. Ed.*, 2007, **46**, 4496–4499.
12. S. Henke, A. Schneemann and R. A. Fischer, *Adv. Funct. Mater.*, 2013, **23**, 5990–5996.
13. L. E. Kreno, K. Leong, O. K. Farha, M. Allendorf, R. P. Van Duyne and J. T. Hupp, *Chem. Rev.*, 2012, **112**, 1105–1125.
14. E. Coronado, M. Giménez-Marqués, G. M. Espallargas and L. Brammer, *Nat. Commun.*, 2012, **3**, 828.
15. E. Coronado and G. Mínguez Espallargas, *Chem. Soc. Rev.*, 2013, **42**, 1525.
16. S. Horike, S. Shimomura and S. Kitagawa, *Nat. Chem.*, 2009, **1**, 695–704.
17. M. A. C. Stuart, W. T. S. Huck, J. Genzer, M. Müller, C. Ober, M. Stamm, G. B. Sukhorukov, I. Szleifer, V. V. Tsukruk, M. Urban, F. Winnik, S. Zauscher, I. Luzinov and S. Minko, *Nat. Mater.*, 2010, **9**, 101–113.
18. Y. Sakata, S. Furukawa, M. Kondo, K. Hirai, N. Horike, Y. Takashima, H. Uehara, N. Louvain, M. Meilikhov, T. Tsuruoka, S. Isoda, W. Kosaka, O. Sakata and S. Kitagawa, *Science*, 2013, **339**, 193–196.
19. M. Ogawa, T. Ishii, N. Miyamoto and K. Kuroda, *Adv. Mater.*, 2001, **13**, 1107–1109.
20. N. Iyi, T. Fujita, C. V. Yelamaggad and F. Lopez Arbeloa, *Appl. Clay Sci.*, 2001, **19**, 47–58.
21. T. Yamamoto, Y. Umemura, O. Sato and Y. Einaga, *Chem. Mater.*, 2004, **16**, 1195–1201.
22. H. Heinz, R. A. Vaia, H. Koerner and B. L. Farmer, *Chem. Mater.*, 2008, **20**, 6444–6456.
23. Y. Nabetani, H. Takamura, Y. Hayasaka, S. Sasamoto, Y. Tanamura, T. Shimada, D. Masui, S. Takagi, H. Tachibana, Z. Tong and H. Inoue, *Nanoscale*, 2013, **5**, 3182–3193.
24. U. Costantino, N. Coletti, M. Nocchetti, G. G. Aloisi and F. Elisei, *Langmuir*, 1999, **15**, 4454–4460.
25. L. Latterini, M. Nocchetti, G. G. Aloisi, U. Costantino and F. Elisei, *Inorganica*

Chim. Acta, 2007, **360**, 728–740.
26. Y. Nabetani, H. Takamura, Y. Hayasaka, T. Shimada, S. Takagi, H. Tachibana, D. Masui, Z. Tong and H. Inoue, *J. Am. Chem. Soc.*, 2011, **133**, 17130–17133.
27. F. Leroux and C. Taviot-Guého, *J. Mater. Chem.*, 2005, **15**, 3628.
28. S. M. Auerbach, K. A. Carrado and P. K. Dutta, *Handbook of Layered Materials*, CRC Press, 2004.
29. D. Yan, J. Lu, M. Wei, D. G. Evans and X. Duan, *J. Mater. Chem.*, 2011, **21**, 13128.
30. G. Abellán, J. A. Carrasco and E. Coronado, *Inorg. Chem.*, 2013, **52**, 7828–7830.
31. G. Abellan, J. A. Carrasco, E. Coronado, J. Romero and M. Varela, *J. Mater. Chem. C*, 2014, **2**, 3723–3731.
32. E. Coronado, J. R. Galán-Mascarós, C. Mart Gastaldo, A. Ribera, E. Palacios, M. Castro and R. Burriel, *Inorg. Chem.*, 2008, **47**, 9103–9110.
33. G. Abellán, E. Coronado, C. Martí-Gastaldo, A. Ribera, J. L. Jordá and H. García, *Adv. Mater.*, 2014, **26**, 4156–4162.
34. S. Cadars, G. Layrac, C. Gérardin, M. Deschamps, J. R. Yates, D. Tichit and D. Massiot, *Chem. Mater.*, 2011, **23**, 2821–2831.
35. G. Abellán, E. Coronado, C. Martí-Gastaldo, J. Waerenborgh and A. Ribera, *Inorg. Chem.*, 2013, **52**, 10147–10157.
36. X. Wang, J. Lu, W. Shi, F. Li, M. Wei, D. G. Evans and X. Duan, *Langmuir*, 2010, **26**, 1247–1253.
37. S.-M. Xu, S.-T. Zhang, W.-Y. Shi, F.-Y. Ning, Y. Fu and H. Yan, *RSC Adv*, 2014, **4**, 47472–47480.
38. M. Ogawa and M. Hiramine, *Cryst. Growth Des.*, 2014, **14**, 1516–1519.
39. Z. Sekkat and W. Knoll, *Photoreactive Organic Thin Films*, Academic Press, 2002.
40. G. Abellán, H. García, C. J. Gómez-García and A. Ribera, *J. Photochem. Photobiol. Chem.*, 2011, **217**, 157–163.
41. H. M. D. Bandara and S. C. Burdette, *Chem. Soc. Rev.*, 2012, **41**, 1809–1825.
42. X. Duan and D. G. Evans, *Layered Double Hydroxides*, Springer, 2006.
43. S. Ishihara, N. Iyi, Y. Tsujimoto, S. Tominaka, Y. Matsushita, V. Krishnan, M. Akada, J. Labuta, K. Deguchi, S. Ohki, M. Tansho, T. Shimizu, Q. Ji, Y. Yamauchi, J. P. Hill, H. Abe and K. Ariga, *Chem. Commun.*, 2013, **49**, 3631–3633.
44. J. Demel, J. Hynek, P. Kovář, Y. Dai, C. Taviot-Gueho, O. Demel, M. Pospíšil and K. Lang, *J. Phys. Chem. C*, 2014, 141024092735001.
45. F. W and A. K, *J. Am. Chem. Soc.*, 1997, **119**, 4563–4564.
46. Y. Einaga, O. Sato, T. Iyoda, A. Fujishima and K. Hashimoto, *J. Am. Chem. Soc.*, 1999, **121**, 3745–3750.
47. J. Pérez-Ramírez, A. Ribera, F. Kapteijn, E. Coronado and C. J. Gómez-García, *J. Mater. Chem.*, 2002, **12**, 2370–2375.
48. C. J. Wang, Y. A. Wu, R. M. J. Jacobs, J. H. Warner, G. R. Williams and D. O'Hare, *Chem. Mater.*, 2011, **23**, 171–180.
49. C. Chakraborty, K. Dana and S. Malik, *J. Phys. Chem. C*, 2011, **115**, 1996–2004.
50. J. Han, D. Yan, W. Shi, J. Ma, H. Yan, M. Wei, D. G. Evans and X. Duan, *J. Phys. Chem. B*, 2010, **114**, 5678–5685.
51. U. Costantino, F. Marmottini, M. Nocchetti and R. Vivani, *Eur. J. Inorg. Chem.*, 1998, **1998**, 1439–1446.

52. N. Iyi, T. Matsumoto, Y. Kaneko and K. Kitamura, *Chem. Mater.*, 2004, **16**, 2926–2932.

FIGURES:

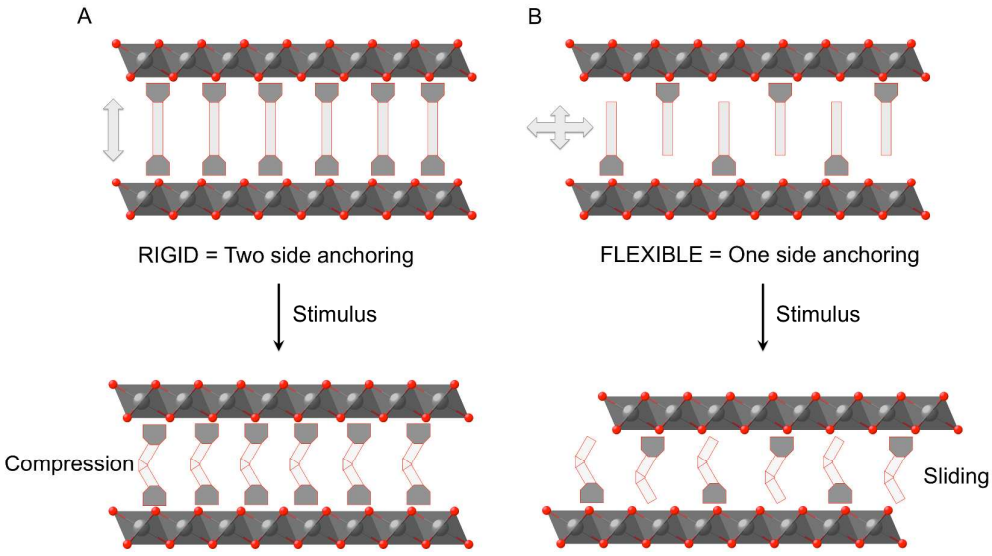

Figure 1. Schematic diagram of the LDH nanosheets compression/sliding movement and interlayer distance change by application of an external stimulus to: (A) a rigid system consisting on two side anchoring molecules acting as molecular bridges; and (B) a more flexible one having only one anchoring group.

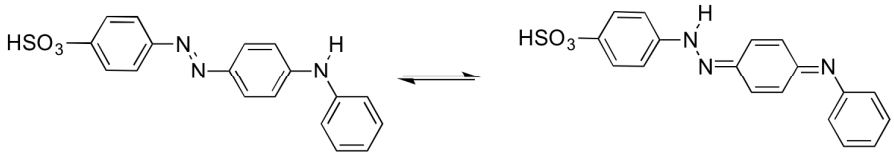

Figure 2. Tautomeric equilibrium between the *A*– and the *H*–form of the 4-(4-anilinophenylazo)benzenesulfonate.

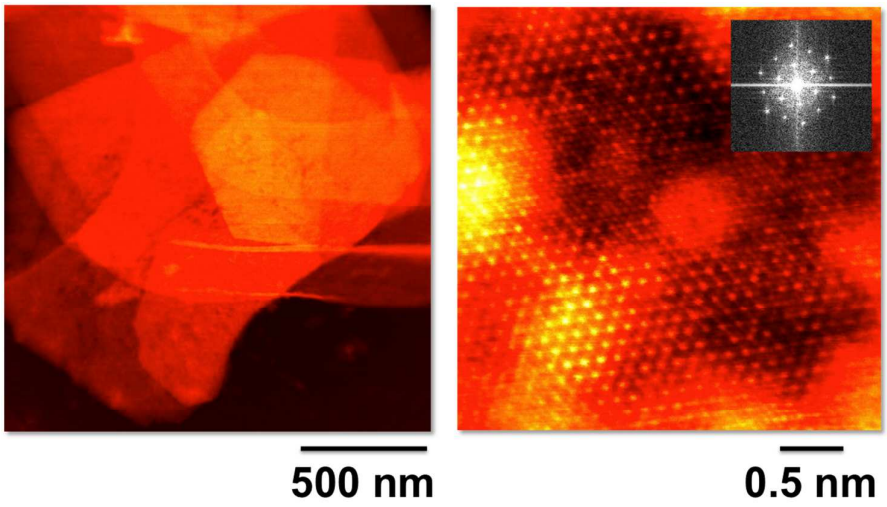

Figure 3. (*left*) Low magnification image of the platelets, which are 500–1000 nm in size. (*right*) High magnification HAADF image. The inset shows the image fast Fourier transform, which exhibits the hexagonal symmetry of the crystal.

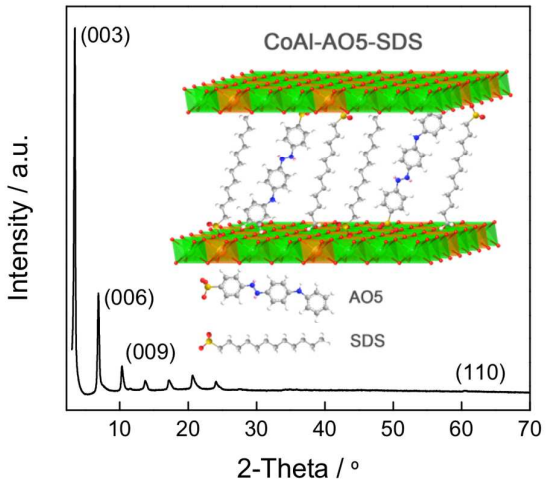

Figure 4. X-ray diffraction pattern of CoAl–AO5.

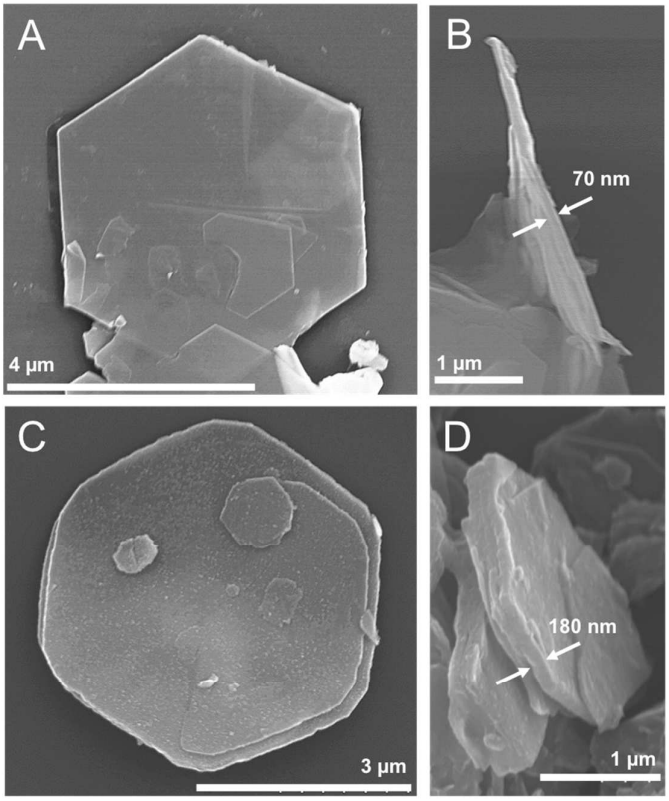

Figure 5. FESEM images of the CoAl–NO_3 (A and B) and CoAl–AO5 (C and D) samples, showing hexagonal well-defined morphology and their thickness.

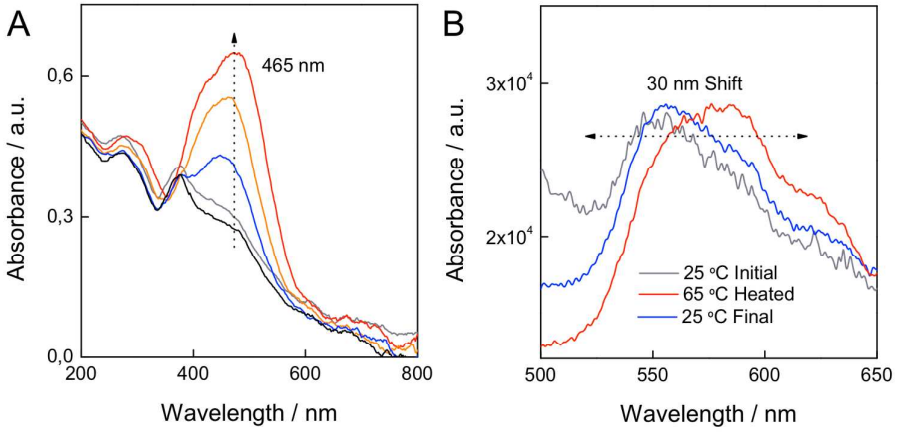

Figure 6. (A) In-situ transmission absorption spectra of the CoAl–AO5 film during heating in the temperature range 25−80 °C. (B) The corresponding in-situ fluorescence spectra showing the reversible peak shift after heating at 65 ºC.

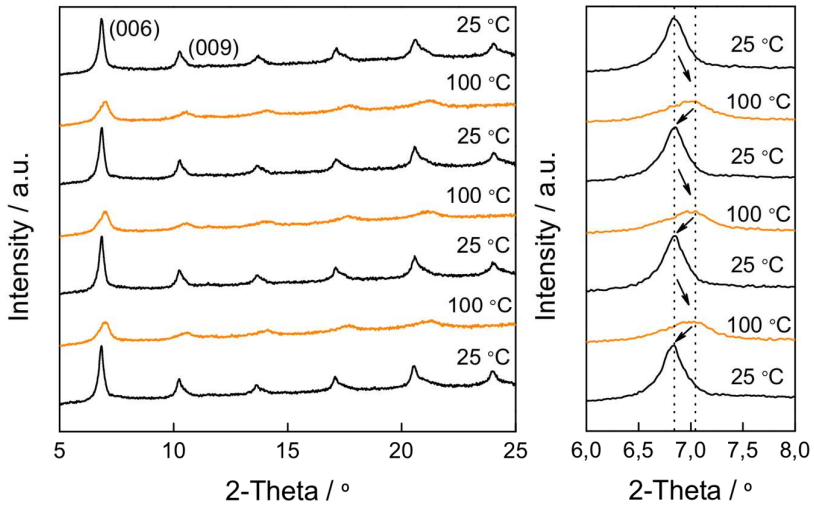

Figure 7. The reversible change in the XRD pattern of CoAl–AO5 upon heating and cooling. The zoom in highlights the movement and broadness increase of the (006) peak.

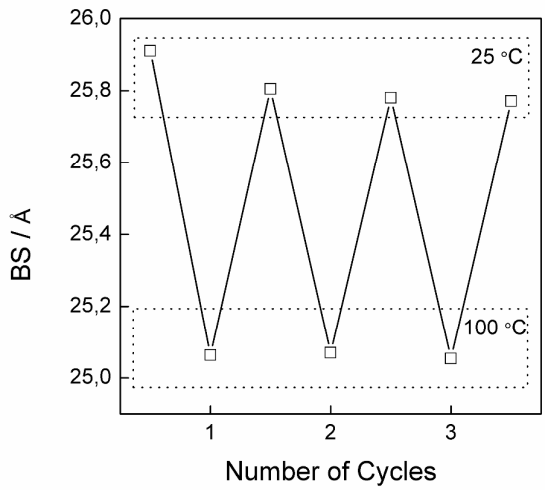

Figure 8. The variation of the basal space during several cycles of heating and cooling.

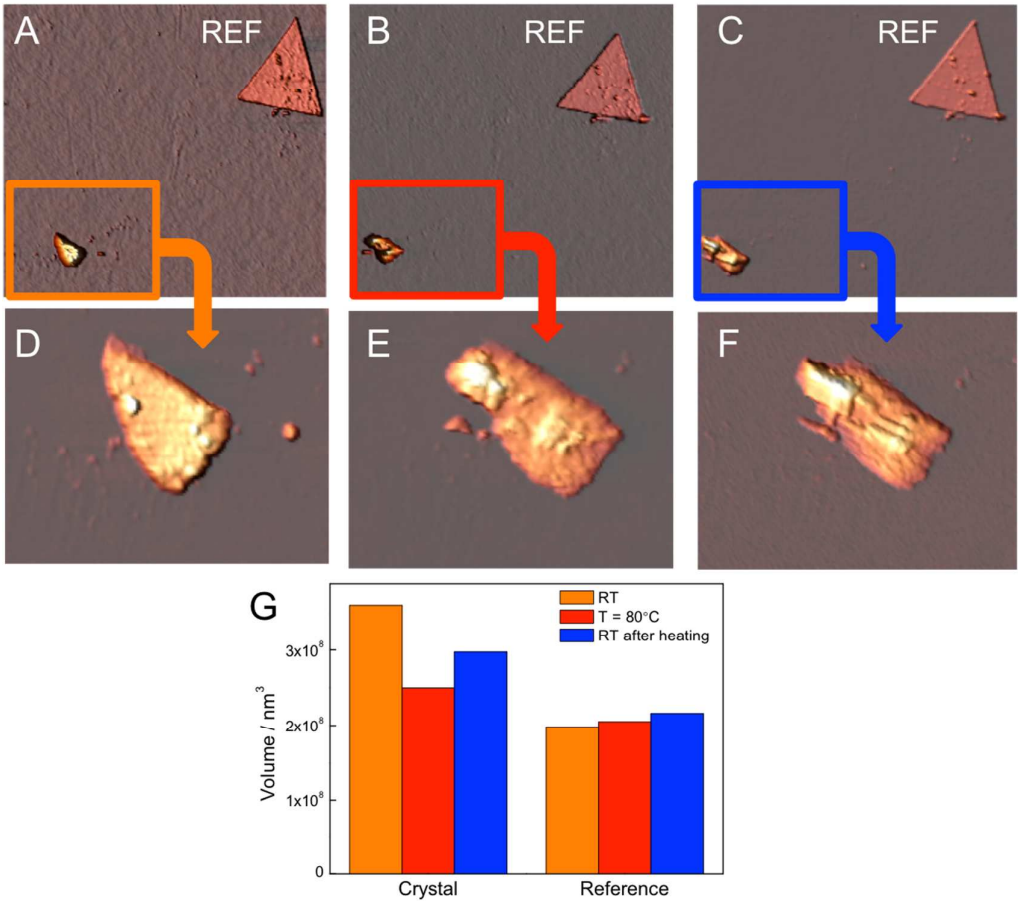

Figure 9. AFM images of CoAl–AO5 acquired at ambient conditions and different temperatures. In each image we can distinguish a crystal and a reference marker: (A) RT; (B) 80ºC; (C) RT after heating the sample at 80 ºC. Images size: 17 µm x 17 µm. (D), (E) and (F) corresponds to zooms of (A), (B), (C) images to observe in detail the evolution of the shape of the crystal. (g) Histogram of the volume of CoAl–AO5 and the reference measured by AFM.

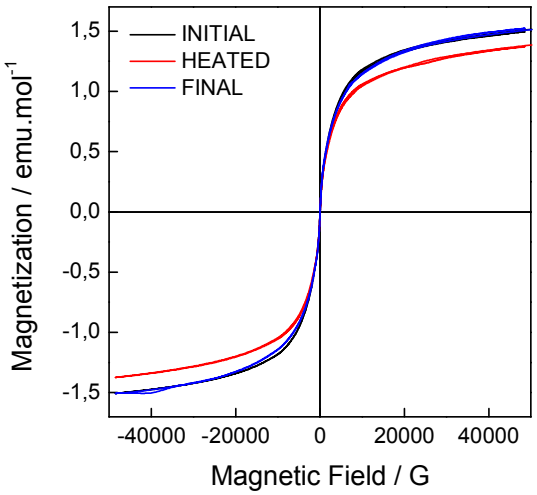

Figure 10. Hysteresis cycles for the initial CoAl–AO5 (black), and the corresponding heated (red) and final (blue) samples.